

Forecasting the U.S. Renewable-Energy Mix with an ALR-BDARMA Compositional Time-Series Framework

Harrison Katz^{*1} and Thomas Maierhofer²

¹Forecasting, Data Science, Airbnb

²Department of Statistics and Data Science, UCLA

Abstract

Accurate forecasts of the U.S. renewable-generation mix are essential for planning transmission upgrades, sizing storage, and setting balancing-market rules. We introduce a Bayesian Dirichlet ARMA model (BDARMA) tailored to monthly shares of hydro, geothermal, solar, wind, wood, municipal waste, and biofuels from January 2010 through January 2025. The mean vector is modeled with a parsimonious VAR(2) in additive-log-ratio space, while the Dirichlet concentration parameter follows an intercept plus ten Fourier harmonics, allowing seasonal widening and narrowing of predictive dispersion.

Forecast performance is assessed with a 61-split rolling-origin experiment that issues twelve-month density forecasts from January 2019 to January 2024. Compared with three alternatives—a Gaussian VAR(2) fitted in transform space, a seasonal naïve that repeats last year’s proportions, and a drift-free ALR random walk—BDARMA lowers the mean continuous-ranked probability score by 15–60 %, achieves component-wise 90 % interval coverage near nominal, and maintains point accuracy (Aitchison RMSE) on par with the Gaussian VAR through eight months and within 0.02 units afterward. These results highlight BDARMA’s ability to deliver sharp, well-calibrated probabilistic forecasts for multivariate renewable-energy shares without sacrificing point precision.

Keywords: compositional time series; Dirichlet state-space; Bayesian forecasting; renewable-energy mix; seasonality.

1 Introduction

Electric-sector decarbonization hinges not only on expanding renewable output but also on anticipating *how the mix of generation technologies will evolve*. Hydropower, wind,

^{*}Correspondence: harrison.katz@airbnb.com

solar, biomass and geothermal differ sharply in marginal cost, intermittency and siting constraints; reliable medium-term *mix forecasts* therefore shape transmission expansion, storage sizing and market design (International Energy Agency, 2024; U.S. Energy Information Administration, 2024; U.S. Energy Information Administration, 2025). Renewables already supply about one-fifth of U.S. utility-scale electricity and their share is expected to double before 2050, making the coherence and accuracy of share forecasts more important than ever.

Why compositional methods? Shares are *compositional*: they are bounded between zero and one and must sum to unity. Forecasting each component in isolation, as is common with univariate ARIMA or machine-learning regressions (Panapakidis and Dagoumas, 2016; Chen et al., 2017), yields incoherent predictions that may turn negative or exceed 100% (Hyndman and Athanasopoulos, 2018). Aitchison’s log-ratio geometry provides a principled fix (Aitchison, 1986). Early multivariate illustrations, such as the VAR for geological compositions in Billheimer et al. (2001), and the state-space model of Snyder et al. (2017), demonstrate that standard Gaussian machinery works once data are mapped to real space. Still, Gaussian log-ratio models often overstate predictive dispersion and ignore seasonally varying volatility.

Simplex-native likelihoods. Recent research therefore models the composition itself. A Dirichlet ARMA process was proposed by Zheng et al. (2017), a dynamic Dirichlet–multinomial filter by Koopman et al. (2023), and a deep hierarchical Dirichlet forecaster by Das et al. (2023). In the cross-sectional domain, Morais et al. (2018) show that Dirichlet and compositional regression can outperform traditional attraction models when explaining brand market shares, underscoring the versatility of simplex-based methods. A direct antecedent to the present study is the Bayesian Dirichlet ARMA (BDARMA) framework introduced by Katz et al. (2024), and subsequently explored with shrinkage priors for trading-sector shares by Katz et al. (2025), which we adopt here as the data model for a new application to the U.S. renewable-energy mix.

Evidence from energy studies. Applications to energy shares remain limited but growing. Compositional VAR and ARMA models, and more recently regional optimization studies, have been used to project national and sub-national energy structures in China, the USA and Canada (Wei et al., 2021; He et al., 2022; Xu et al., 2024; Xiao and Li, 2023). Grey-system and hybrid approaches, such as adaptive discrete grey models and MGM–BPNN–ARIMA designs for broad-mix or bio-energy forecasting, further boost accuracy while respecting the simplex constraint (Qian et al., 2022; Zhang et al., 2022; Suo et al., 2024). Machine-learning work such as the LSTM study by Ma et al. (2018) and logistic growth analysis of U.S. energy trajectories by Harris et al. (2018) underline the need to tame nonlinearities, but they still rely on ad-hoc renormalization.

Contribution. We apply the Bayesian Dirichlet ARMA framework to the seven-component U.S. renewable-energy mix measured monthly from 2010 to 2024, a data set with pronounced seasonality and secular trends hitherto unaddressed in the Dirichlet literature. Forecast skill is benchmarked against three alternatives: a Gaussian VAR(2) in additive-log-ratio space with identical Fourier dummies, a seasonal naïve that repeats the mix observed twelve months earlier, and a drift-free ALR random walk. A 61-split rolling protocol produces 732 out-of-sample density forecasts and shows that the Dirichlet model attains the lowest continuous-ranked probability score at every horizon while matching the VAR’s point accuracy. A full-sample forecast issued in January 2025 encloses a trajectory where wind and solar exceed one-third of renewable generation by early 2026, with credible bands roughly half as wide as those implied by the VAR—information directly relevant for transmission and storage planning.

The remainder of the paper is organized as follows. Section 2 describes the EIA data and seasonal covariates. Section 3 presents the BDARMA and benchmark models. Section 4 details the rolling evaluation protocol and scoring rules. Results are discussed in Section 5, and Section 6 concludes with policy implications and avenues for future research.

2 Data

The empirical analysis relies on the EIA monthly *renewable-energy consumption* data set. We retain $T = 181$ consecutive months from January 2010 through January 2025. Each observation is a seven-part composition $\mathbf{y}_t = (y_{t,\text{hyd}}, y_{t,\text{geo}}, y_{t,\text{sol}}, y_{t,\text{win}}, y_{t,\text{woo}}, y_{t,\text{was}}, y_{t,\text{bio}})^\top \in \mathcal{S}_7$, where shares are obtained by dividing each raw series by their monthly total.

Additive-log-ratio (ALR) coordinates. Throughout we analyse the seven-part composition in *additive-log-ratio* form

$$\mathbf{e}_t = \text{alr}(\mathbf{y}_t) = (\log \frac{y_{t,\text{hyd}}}{y_{t,\text{bio}}}, \log \frac{y_{t,\text{geo}}}{y_{t,\text{bio}}}, \log \frac{y_{t,\text{sol}}}{y_{t,\text{bio}}}, \log \frac{y_{t,\text{win}}}{y_{t,\text{bio}}}, \log \frac{y_{t,\text{woo}}}{y_{t,\text{bio}}}, \log \frac{y_{t,\text{was}}}{y_{t,\text{bio}}})^\top \in \mathbb{R}^6, \quad (1)$$

where *biofuels* serve as the common denominator (reference part). The inverse map $\text{alr}^{-1} : \mathbb{R}^6 \rightarrow \mathcal{S}_7$ restores a share vector via $y_{t,j} = \exp(e_{t,j}) \left[1 + \sum_{k=1}^6 \exp(e_{t,k}) \right]^{-1}$ for $j \leq 6$ and $y_{t,\text{bio}} = \left[1 + \sum_{k=1}^6 \exp(e_{t,k}) \right]^{-1}$. We write $e_{t,j}$ for the j -th ALR coordinate and collect them as e_1, \dots, e_6 when no time index is needed.

2.1 Exploratory data analysis

Figure 1 highlights two macro-patterns in the sample: (i) pronounced, asymmetric intra-annual seasonality and (ii) a medium-run reallocation of market share from hydro to wind and solar.

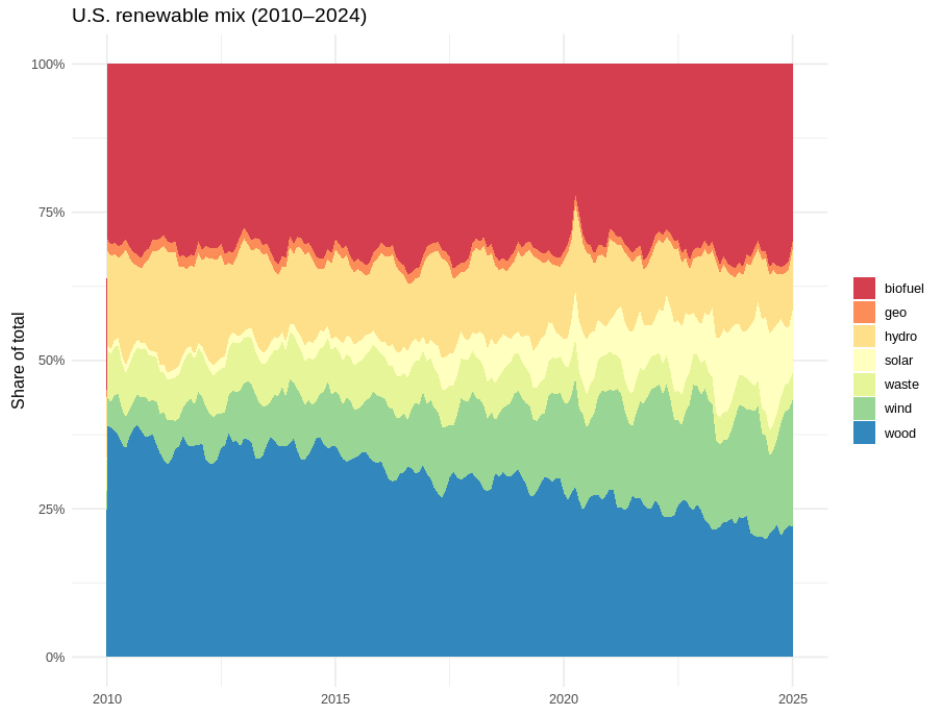


Figure 1: Monthly U.S. renewable-energy mix, 2010–2025. Hydro loses ground, while wind and solar expand rapidly. Seasonality is most pronounced in hydro (spring runoff) and wind (winter–spring peak). Areas are stacked so each month sums to 100%.

Seasonality. Panel (a) of Figure 2 shows component-wise box plots of monthly shares for 2010–2024; panel (b) traces the mean intra-year profile. Hydro exhibits the largest seasonal swing, peaking in April–May and troughed in late summer while wind follows a bimodal winter/autumn pattern and solar the mirror image with a July plateau. Biomass, geothermal and waste are comparatively flat, with median intra-year movements below 1 pp.

Cross-source dependence. Figure 3(a) plots the correlation matrix of the six ALR coordinates e_1, \dots, e_6 (biofuels as reference). Solar and wind move almost one-for-one relative to biofuels ($\rho_{e_5, e_6} = 0.97$), whereas hydro and wind are strongly anti-correlated ($\rho \approx -0.86$). Panel (b) confirms these pair-wise relations are non-linear, displaying the characteristic banana-shaped clouds induced by log-ratio geometry.

Distributional heterogeneity. Table 1 shows wide dispersion differences: hydro ranges from 7.5% to 20.3% (SD = 2.6 pp), geothermal is quasi-deterministic (SD = 0.17 pp) and wood the most volatile component (SD = 5.1 pp).

Lag-order diagnostics. To determine the minimum dynamic order in ALR space we fitted VAR(1) and VAR(2) models and applied Ljung–Box and Hosking portmanteau tests to the residuals (Table 2). A Ljung–Box residual diagnostic rejects the white-noise null for coordinate e_3 under VAR(1) ($p < 0.001$), whereas no coordinate is rejected under VAR(2) (smallest p-value=.14). The residual ACF panels in Figure 4 show that the prominent spikes at lags 1–2 present under VAR(1) vanish when the second lag is added. At the system level, the portmanteau statistic at horizon 12 remains marginally significant; adding centered monthly dummies reduces χ^2 from 628 to 431 ($p = 0.006$). Because VAR(2) is the *smallest* specification to clear all short-run autocorrelation and further lags inflate the parameter count without material gain, we adopt a VAR(2) mean and address any residual seasonality through exogenous Fourier terms.

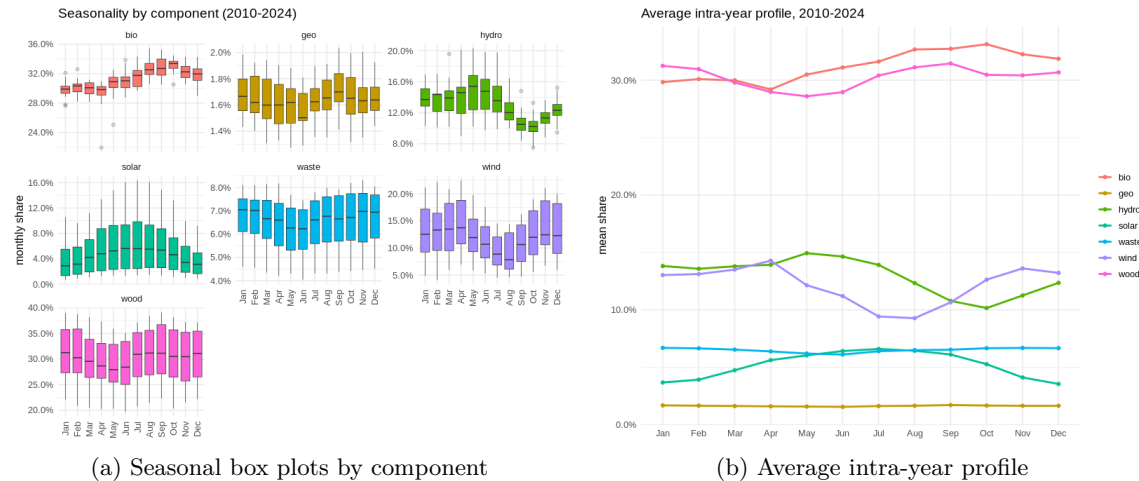


Figure 2: Seasonal variation in renewable-energy shares, 2010–2024. Boxes span the inter-quartile range; black bars mark the median. Means in panel (b) highlight opposing hydro/solar and hydro/wind peaks.

Because the data exhibit markedly different seasonal amplitudes, strong yet uneven cross-correlations, and component-specific dispersion and because the residual diagnostics show that two lags are the minimum needed for whiteness, we adopt a specification built on three mutually reinforcing elements: a second-order vector autoregressive mean in ALR space to capture short-run dynamics, a single seasonal precision curve that modulates uncertainty across the calendar year for every component, and a Dirichlet likelihood that both imposes the compositional sum-to-one constraint and allows each source’s variance to remain distinct.

Software environment. All computations were carried out in R 4.3.2 (R Core Team, 2024) with Stan 2.33 via the `rstan` interface (Goodrich et al., 2024; Stan Development

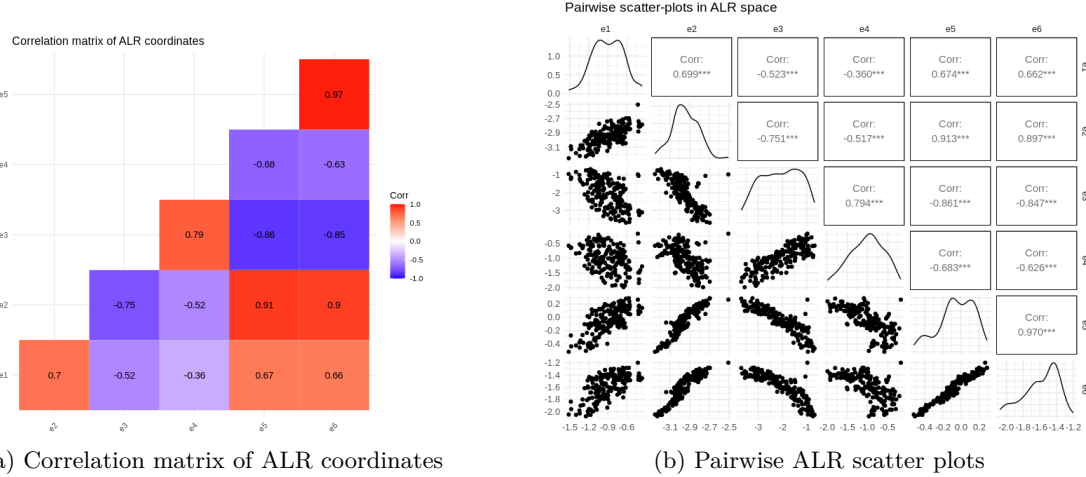


Figure 3: Cross-source dependence in additive-log-ratio space. Positive (red) and negative (blue) correlations in panel (a) exceed 0.9 in absolute magnitude; scatter plots in panel (b) reflect the non-linear shape induced by the simplex geometry.

Team, 2023). Data wrangling, graphics and tables relied on **tidyverse** (Wickham et al., 2019), **lubridate** (Grolemund and Wickham, 2011), **janitor** (Firke, 2023), **scales** (Wickham and Seidel, 2019), **patchwork** (Pedersen, 2025), **ggcorrplot** (Kassambara, 2022), **GGally** (Di Cook et al., 2021) and **kableExtra** (Zhu, 2021). Compositional methods used **compositions** (van den Boogaart and Tolosana-Delgado, 2024) and the **transport** package for Aitchison norms (Schuhmacher et al., 2020). Time-series estimation and testing employed **vars** (Pfaff, 2008), **FinTS** (Pfaff, 2024) and **MTS** (Tsay, 2023).

3 Forecasting model

Let the monthly renewable-energy mix be the $J=7$ -component composition

$$\mathbf{y}_t = (y_{t,\text{hyd}}, y_{t,\text{geo}}, y_{t,\text{sol}}, y_{t,\text{win}}, y_{t,\text{woo}}, y_{t,\text{was}}, y_{t,\text{bio}})^\top \in \mathcal{S}_7, \quad t = 1, \dots, T.$$

Biofuels ($j^* = 7$) serve as reference part in every additive-log-ratio (ALR) transform that follows.

Dirichlet observation layer. We model \mathbf{y}_t as a Dirichlet distributed whose parameter vector factorizes into a simplex-valued mean $\boldsymbol{\mu}_t$ and a positive precision scalar ϕ_t :

$$y_t \mid \boldsymbol{\mu}_t, \phi_t \sim \text{Dirichlet}(\phi_t \boldsymbol{\mu}_t), \quad \boldsymbol{\mu}_t \in \mathcal{S}_7, \quad \phi_t > 0. \quad (2)$$

Table 1: Component means and dispersion, 2010–2024 (percent of total renewables).

	Hydro	Geo	Solar	Wind	Wood	Waste	Bio
Mean (%)	13.0	1.64	5.20	12.2	30.3	6.51	31.2
SD (%)	2.63	0.17	3.87	4.65	5.10	1.15	1.86
Q1 (%)	10.9	1.50	1.91	8.48	26.4	5.54	30.1
Q3 (%)	14.8	1.77	7.53	15.1	35.1	7.48	32.5
Min (%)	7.51	1.28	0.73	4.18	19.7	4.05	22.0
Max (%)	20.3	2.03	16.3	22.5	39.1	8.31	35.4

Table 2: Residual diagnostic statistics (lags 1–2 for Ljung–Box, horizon 12 for Hosking portmanteau).

Model	Test	e_1	e_2	e_3	e_4	e_5	e_6
VAR(1)	Ljung–Box p	0.99	0.79	0.00	0.08	0.49	0.20
VAR(2)	Ljung–Box p	0.99	0.98	0.47	0.73	0.57	0.14
Portmanteau χ^2 / p		628	/	< 0.001	(VAR(2))		

Mean vector in ALR space. Let $\boldsymbol{\eta}_t = \text{alr}(\boldsymbol{\mu}_t) \in \mathbb{R}^{J-1}$; for $J = 7$ this is a six-vector $\boldsymbol{\eta}_t = (\eta_{t1}, \dots, \eta_{t6})^\top$ of log-ratios against biofuels. Its inverse is

$$\mu_{tj} = \frac{\exp(\eta_{tj})}{1 + \sum_{k=1}^6 \exp(\eta_{tk})} \quad (j \leq 6), \quad \mu_{t,7} = \left[1 + \sum_{k=1}^6 \exp(\eta_{tk}) \right]^{-1}.$$

Seasonal precision curve. Calendar variation in forecast dispersion is captured by letting the log-precision depend on an intercept and ten Fourier harmonics:

$$\log \varphi_t = \mathbf{f}_t^\top \boldsymbol{\gamma}, \quad \mathbf{f}_t = (1, \mathbf{g}_t^\top)^\top, \quad \mathbf{g}_t = \left(\sin \frac{2\pi t}{12}, \cos \frac{2\pi t}{12}, \dots, \sin \frac{10\pi t}{12}, \cos \frac{10\pi t}{12} \right)^\top, \quad \boldsymbol{\gamma} \in \mathbb{R}^{11}. \quad (3)$$

State (mean) dynamics. Short-run cross-technology interactions are modelled with a second-order vector autoregression process in ALR space:

$$\boldsymbol{\eta}_t = \mathbf{X}_t \boldsymbol{\beta} + \mathbf{A}_1 (\boldsymbol{\eta}_{t-1} - \mathbf{X}_{t-1} \boldsymbol{\beta}) + \mathbf{A}_2 (\boldsymbol{\eta}_{t-2} - \mathbf{X}_{t-2} \boldsymbol{\beta}), \quad \mathbf{X}_t = I_{J-1} \otimes \mathbf{f}_t^\top, \quad (4)$$

where (i) $\mathbf{A}_1, \mathbf{A}_2 \in \mathbb{R}^{6 \times 6}$ are AR coefficient matrices; (ii) \mathbf{X}_t block-replicates the 11-vector \mathbf{f}_t across the six ALR coordinates, giving $\mathbf{X}_t \in \mathbb{R}^{6 \times 66}$; and (iii) $\boldsymbol{\beta} \in \mathbb{R}^{66}$ contains component-specific regression slopes for the seasonal dummies.

Geometric preliminaries and evaluation mapping

Let $y_t \in \mathcal{S}_7$ denote the share vector and $e_t = \text{alr}(y_t) \in \mathbb{R}^6$ its additive log-ratio (ALR) coordinates with biofuels as the reference part; alr^{-1} restores shares (see Eq. (1)). We

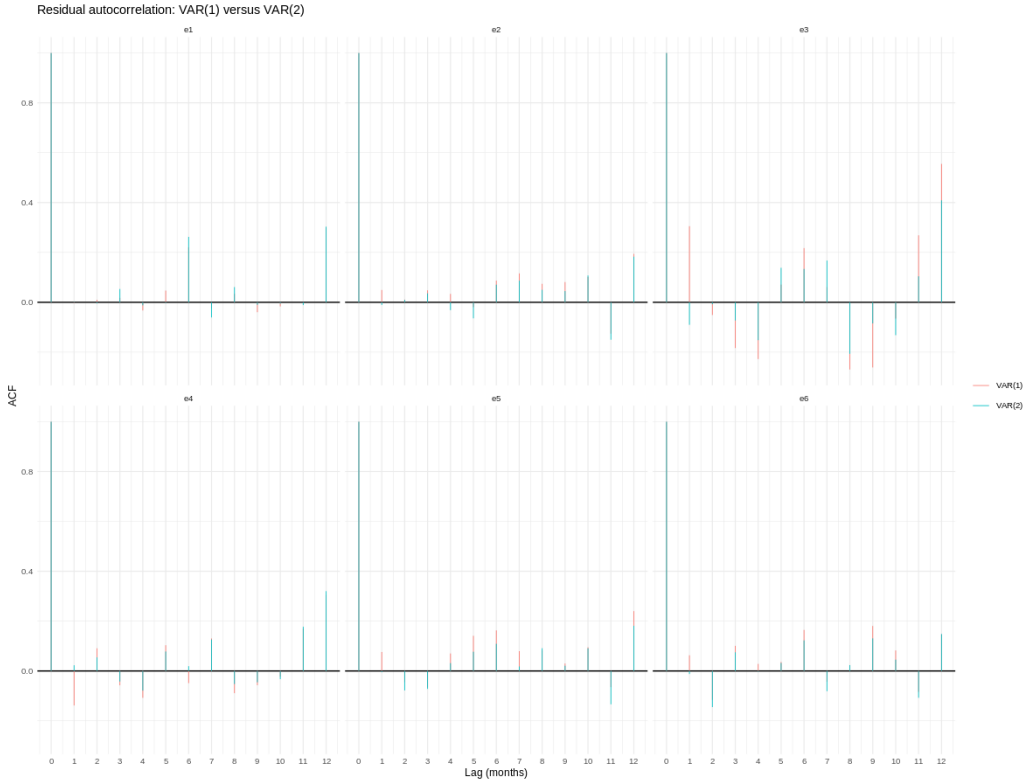


Figure 4: Residual autocorrelation by ALR coordinate: red=VAR(1); blue=VAR(2). Adding the second lag removes the large spikes at lags 1–2.

model the mean in ALR space (Eq. (4)) and obtain *predictive draws in share space* from the Dirichlet observation layer (Eq. (2)). Forecasts are evaluated in two complementary spaces: CRPS in share space for joint sharpness and calibration (Eq. (5)), and clr-based RMSE in Aitchison geometry for point accuracy (Eq. (6)). Because space choice induces different cross-component dependencies, reporting both clarifies where improvements arise. *Reference-free coordinates.* The logistic-normal (sometimes “ALN”) family places a Gaussian law on log-ratio coordinates; the isometric log-ratio (ILR) transform provides orthonormal, reference-free coordinates with full metric equivalence on the simplex (Aitchison and Shen, 1980; Egozcue et al., 2003; Aitchison, 1986). This means that the DARMA data models with these three link functions are equivalent, provided the same transformation is applied to the priors. We retain ALR for interpretability and continuity with Eq. (1).

Prior specification and inference. Each scalar element of $\mathbf{A}_1, \mathbf{A}_2, \boldsymbol{\beta}$ and $\boldsymbol{\gamma}$ receives an independent $\mathcal{N}(0, 1)$ prior. Posterior inference proceeds via Hamiltonian Monte Carlo (four chains; 500 warm-up and 500 retained iterations per chain) in Stan, yielding 2 000

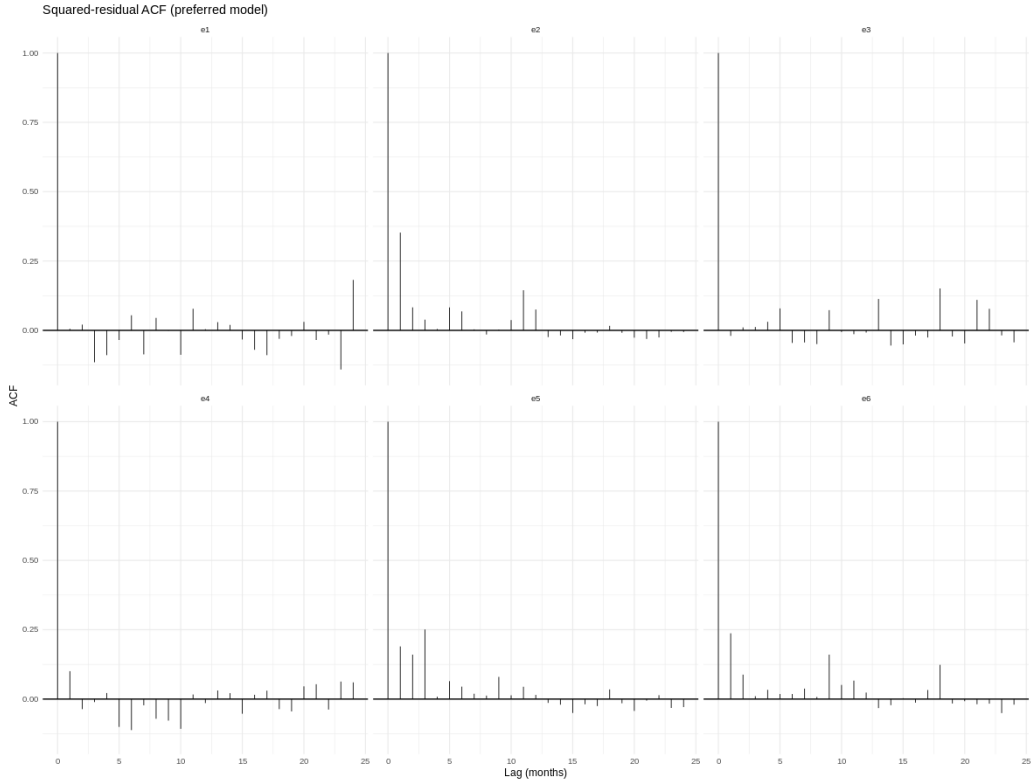


Figure 5: ACF of squared residuals for the preferred VAR(2) + season model. Modest spikes in e_2 and e_5 motivate the component-wise GARCH precision adopted later.

draws that underpin all density-forecast evaluations presented later.

3.1 Transform-space VAR(2) (tVAR(2))

Working in ALR coordinates,

$$\boldsymbol{\eta}_t = \mathbf{F}_1 \boldsymbol{\eta}_{t-1} + \mathbf{F}_2 \boldsymbol{\eta}_{t-2} + \mathbf{X}_t \boldsymbol{\delta} + \boldsymbol{\varepsilon}_t, \quad \boldsymbol{\varepsilon}_t \sim \mathcal{N}(\mathbf{0}, \boldsymbol{\Sigma}).$$

Parameters $(\mathbf{F}_1, \mathbf{F}_2, \boldsymbol{\delta}, \boldsymbol{\Sigma})$ are estimated by ordinary least squares with the same seasonal regressors \mathbf{X}_t . Multi-step forecasts are generated under the Gaussian innovation assumption and mapped back with alr^{-1} .

3.2 Additive-log-ratio random walk (ALR-RW)

A drift-free benchmark sets each future ALR vector equal to the most recent observation: $\boldsymbol{\eta}_{t+h|t} = \boldsymbol{\eta}_t$. Back-transformation yields a single point forecast with zero predictive spread.

3.3 Seasonal naïve copy-last-year (S-NAIVE)

The seasonal naïve copies the composition observed 12 months earlier: $\mathbf{y}_{t+h|t} = \mathbf{y}_{t+h-12}$.

These four specifications exploit the same information set but differ in how they propagate seasonality, cross-technology dependence and uncertainty. Section 4 details the rolling protocol used to compare their point and density-forecast performance.

4 Forecast–evaluation protocol

Model comparison follows an expanding–window, rolling-origin design that mirrors the workflow used by system operators and energy planners. Let τ_s , $s = 1, \dots, S$, denote the final observation included in estimation window s and let H denote the fixed forecast horizon ($H = 12$). The first origin is $\tau_1 = 2019-01$ and the last origin that still admits a twelve-step look-ahead is $\tau_S = 2024-01$, so $S = 61$. At origin s the estimation set is $\{\mathbf{y}_t : 1 \leq t \leq \tau_s\}$ while the verification set comprises $\{\mathbf{y}_{\tau_s+h} : h = 1, \dots, H\}$.

4.1 Generating predictive distributions

All four competitors are evaluated on Monte-Carlo samples of equal size $M = 2,000$ so that scoring rules are comparable.

BDARMA. For every origin s we retain the M posterior draws $\{\boldsymbol{\theta}^{(m)}\}_{m=1}^M$ returned by the Hamiltonian Monte-Carlo sampler. Each draw is propagated through the deterministic state equation (4) for $h = 1:H$ steps, producing the latent mean $\boldsymbol{\mu}_{s,h}^{(m)}$; a single realization $\mathbf{y}_{s,h}^{(m)} \sim \text{Dirichlet}(\phi_{s,h}^{(m)} \boldsymbol{\mu}_{s,h}^{(m)})$ is then generated from the observation density (2). The empirical set $\mathcal{P}_{s,h}^{\text{BDARMA}} = \{\mathbf{y}_{s,h}^{(m)}\}_{m=1}^M$ constitutes the predictive distribution.

tVAR(2). Let $\hat{\boldsymbol{\eta}}_{s,h}$ and $\hat{\mathbf{V}}_{s,h}$ be, respectively, the conditional mean and covariance of the Gaussian forecast for the ALR vector at horizon h . We draw $\boldsymbol{\eta}_{s,h}^{(m)} \sim \mathcal{N}(\hat{\boldsymbol{\eta}}_{s,h}, \hat{\mathbf{V}}_{s,h})$, transform with alr^{-1} , and obtain $\mathcal{P}_{s,h}^{\text{tVAR}} = \{\text{alr}^{-1}(\boldsymbol{\eta}_{s,h}^{(m)})\}_{m=1}^M$. Because the back-transformation preserves the unit sum.

ALR random walk (ALR–RW). The point forecast is the last observed ALR vector $\boldsymbol{\eta}_{s,0}$. To give the model a distribution that can be scored with CRPS we set $\boldsymbol{\eta}_{s,h}^{(m)} = \boldsymbol{\eta}_{s,0}$ for every m and define $\mathcal{P}_{s,h}^{\text{RW}} = \{\text{alr}^{-1}(\boldsymbol{\eta}_{s,0})\}_{m=1}^M$. The resulting cloud is degenerate but has the same cardinality M .

Seasonal naïve (S-NAIVE). For each horizon h we copy the composition observed exactly one year earlier, \mathbf{y}_{s-12+h} . As with the random walk we replicate this deterministic vector M times, $\mathcal{P}_{s,h}^{\text{S-NAIVE}} = \{\mathbf{y}_{s-12+h}\}_{m=1}^M$.

4.2 Scoring rules

Denote by $\mathbf{y}_{s,h}$ the realized share vector at lead h originating from window s . Two proper scoring rules are applied.

Continuous-ranked probability score. Writing $\|\mathbf{a}\|_1 = \sum_{j=1}^7 |a_j|$ for the ℓ_1 norm, the sample-based estimator is

$$\text{CRPS}_{s,h}(\mathcal{P}) = \frac{1}{M} \sum_{m=1}^M \|\mathbf{y}_{s,h}^{(m)} - \mathbf{y}_{s,h}\|_1 - \frac{1}{2M^2} \sum_{m=1}^M \sum_{m'=1}^M \|\mathbf{y}_{s,h}^{(m)} - \mathbf{y}_{s,h}^{(m')}\|_1, \quad (5)$$

where \mathcal{P} denotes the empirical draw set for the model in question. The CRPS integrates the Brier score over all threshold events inside the simplex and is measured in share points.

Aitchison root-mean-square error. Let $\hat{\boldsymbol{\mu}}_{s,h} = M^{-1} \sum_m \mathbf{y}_{s,h}^{(m)}$ be the posterior mean. With the centred log-ratio $\text{clr}(\mathbf{p}) = (\log p_1/g, \dots, \log p_7/g)$ and geometric mean $g = (\prod_{j=1}^7 p_j)^{1/7}$, the point-forecast error is

$$\text{RMSE}_{s,h} = \|\text{clr}(\mathbf{y}_{s,h}) - \text{clr}(\hat{\boldsymbol{\mu}}_{s,h})\|_2 / \sqrt{7}. \quad (6)$$

Both (5) and (6) reduce to zero for a perfect forecast.

Interval diagnostics. For BDARMA the 5-th and 95-th sample quantiles define a 90 % credible interval for each component. Coverage is tallied over all (s, h) pairs.

4.3 Fixed-origin projection

After the rolling study a single fixed-origin forecast is produced from the complete estimation window 2010-01 – 2025-01 ($\tau^* = T$). Future Fourier regressors \mathbf{f}_{T+h} are generated deterministically, so the only source of uncertainty is the posterior distribution of model parameters and, for tVAR(2), the Gaussian state noise.

5 Results

5.1 Forecast accuracy across horizons

Table 3 reports the mean continuous-ranked probability score (CRPS) and Table 4 the mean Aitchison root-mean-square error (RMSE) for every horizon; the same information is

visualised in Figures 6 and 7. When scores are aggregated over all sixty-one rolling origins, the Bayesian-Dirichlet ARMA (**BDARMA**) dominates the field. Its mean CRPS at one step ahead is 0.0045, which is roughly one quarter lower than the transform-space VAR(2) (**tVAR(2)**) and more than fifty percent lower than either naïve rule. The advantage widens as the horizon lengthens; by month 12, BDARMA still improves on tVAR(2) by around twenty percent and on the seasonal naïve (**S-NAIVE**) by a factor of 1.4, while the additive-log-ratio random walk (**ALR-RW**) remains the weakest performer throughout.

Point-forecast results tell a complementary story. Up to eight months ahead, BDARMA and tVAR(2) deliver virtually identical RMSEs (Figure 7); thereafter the Gaussian VAR displays a slight numerical edge that peaks at just one-hundredth of an Aitchison unit. That edge, however, is achieved at the cost of substantially wider predictive intervals, as reflected in the persistently higher CRPS. Both naïve rules fare considerably worse: S-NAIVE holds a constant RMSE of about 0.15 and a CRPS that is almost double BDARMA’s, whereas ALR-RW deteriorates sharply until mid-year before converging towards the other benchmarks only because its naive dispersion collapses.

Taken together, these findings underline three practical lessons. First, seasonality matters: the harmonic regressors embedded in f_t provide an immediate and durable boost over models that ignore calendar structure. Second, coherence alone is not enough; although tVAR(2) respects the simplex, its Gaussian scale inflates forecast spread and leaves roughly one-fifth of the potential CRPS improvement on the table. Finally, the Dirichlet precision curve in BDARMA succeeds in producing densities that are simultaneously sharp, well calibrated and competitive in point terms even at the longest horizon considered.

Table 3: Mean CRPS across rolling origins. Boldface marks the best score for each horizon.

Horizon	BDARMA	tVAR(2)	S-NAIVE	ALR-RW
1	0.00449	0.00615	0.0114	0.0086
2	0.00535	0.00740	0.0114	0.0130
3	0.00582	0.00829	0.0115	0.0165
4	0.00617	0.00875	0.0116	0.0183
5	0.00650	0.00928	0.0118	0.0196
6	0.00684	0.00968	0.0119	0.0204
7	0.00713	0.0100	0.0119	0.0201
8	0.00734	0.0102	0.0119	0.0194
9	0.00756	0.0102	0.0119	0.0178
10	0.00783	0.0103	0.0118	0.0153
11	0.00817	0.0105	0.0119	0.0129
12	0.00841	0.0106	0.0120	0.0120

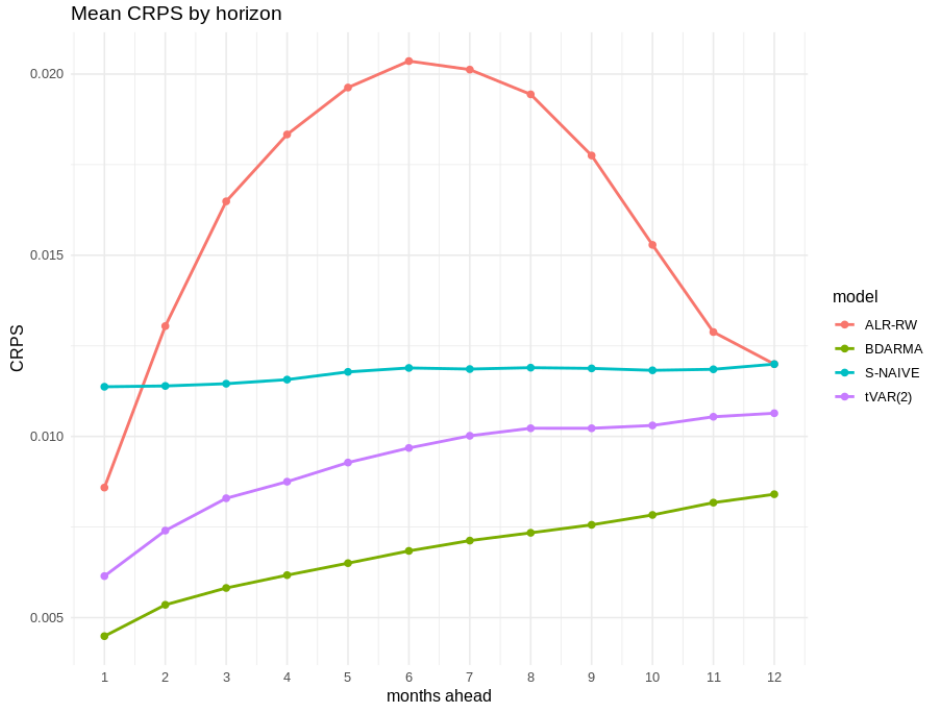


Figure 6: Mean CRPS by horizon, averaged over 61 rolling origins. Lower values indicate sharper and better-calibrated densities.

5.2 Coverage of BDARMA predictive intervals

The Monte-Carlo intervals are well calibrated. Table 5 records the proportion of split-horizon combinations where the realised share vector falls inside the component-wise 90% band. Coverage rises from 86% at one month to 99% at a full year; the geometric ceiling for joint inclusion is 48% at $h = 1$, so the upward trend is expected. Component averages range from 86% for biofuels to 100% for geothermal (Table 6), giving an overall mean of 94.8%.

5.3 Fixed-origin comparison

Figure 8 shows the one-year-ahead trajectories for each technology by model. The central messages are straightforward.

First, BDARMA delivers not only a median path but also a well calibrated 90 % interval. For planners this means that the same forecast set supports both point estimates—needed, for instance, in generation-mix optimization—and a quantification of downside or upside risk that is essential when determining reserve margins, storage dispatch protocols or hedging requirements. The competing methods provide no such density information, forcing

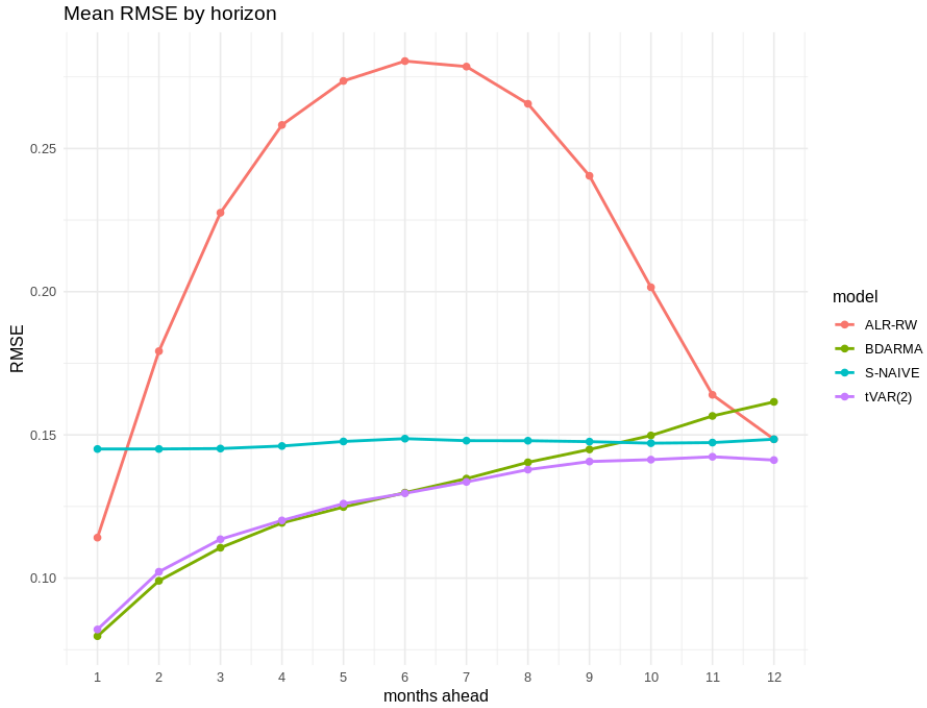


Figure 7: Mean Aitchison RMSE by horizon; lower values indicate more accurate point forecasts.

practitioners to bolt on ad-hoc error bands or run scenario analyses that may or may not respect the unit-sum constraint.

Second, because BDARMA’s concentration parameter is allowed to vary seasonally, the width of its interval changes appreciably across components. High-growth and strongly seasonal sources such as wind and solar retain non-negligible uncertainty, implying that transmission and balancing services must still accommodate significant swings even as their average shares rise. In contrast, geothermal and waste show near-deterministic bands, suggesting that policy targets focused on these technologies can be stated with greater confidence and narrower tolerances.

Third, where the medians diverge the direction is informative in its own right. The harmonic naïve inherits last year’s level and thereby under-projects solar in the presence of an upward trend; the random walk does the opposite by ignoring seasonality entirely; and the Gaussian VAR, although often close to BDARMA in the center, cannot reveal whether any gap that remains is material relative to forecast dispersion. From a policy standpoint this matters when setting technology-specific incentives. Under-estimating solar growth, for example, risks under-sizing flexible resources needed to absorb midday surpluses, whereas over-estimating hydro stability can mask the need for additional spring reserves.

Table 4: Mean Aitchison RMSE across rolling origins. Boldface marks the lowest error at each horizon.

Horizon	BDARMA	tVAR(2)	S-NAIVE	ALR-RW
1	0.0797	0.0821	0.145	0.114
2	0.0990	0.102	0.145	0.179
3	0.111	0.114	0.145	0.228
4	0.119	0.120	0.146	0.258
5	0.125	0.126	0.148	0.274
6	0.130	0.130	0.149	0.281
7	0.135	0.134	0.148	0.279
8	0.140	0.138	0.148	0.266
9	0.145	0.141	0.148	0.240
10	0.150	0.141	0.147	0.202
11	0.157	0.142	0.147	0.164
12	0.162	0.141	0.148	0.148

Table 5: Empirical 90 % coverage of BDARMA component intervals.

h	1	2	3	4	5	6	7	8	9	10	11	12
Cov	.863	.891	.907	.933	.950	.957	.963	.975	.984	.980	.983	.985

6 Conclusion

This study develops and tests a Bayesian Dirichlet ARMA model whose additive-log-ratio mean follows a parsimonious VAR(2) while the Dirichlet concentration parameter evolves with an intercept plus ten monthly harmonics. In a 61-split rolling evaluation the Dirichlet-based approach delivers the sharpest and best-calibrated twelve-month density forecasts for the U.S. renewable-energy mix. Relative to a Gaussian VAR(2) with identical seasonal dummies, mean CRPS falls by roughly one-quarter at short leads and by one-fifth at a full year; gains over both a seasonal naïve and an additive-log-ratio random walk are still larger. Point accuracy measured by Aitchison RMSE is on par with the VAR through eight months and remains within 0.02 units thereafter, underscoring that the improvement is driven by better uncertainty quantification rather than a sacrifice in central tendency.

The single-origin forecast issued for calendar year 2025 illustrates practical implications. BDARMA produces calibrated 90% intervals that tighten for low-volatility sources such as geothermal and waste while remaining wide enough for wind and solar to capture intra-year swings. Because the competing models offer medians only, planners relying on them must add ad-hoc bands or scenario grids that may violate simplex coherence. In contrast, the Dirichlet framework provides a one-stop forecast that can feed directly into capacity-expansion studies, transmission planning, and reliability assessments, all of which

Table 6: Component-wise BDARMA coverage (61×12 forecasts).

Hydro	Geo	Solar	Wind	Wood	Waste	Bio
.939	1.000	.993	.886	.954	.998	.862

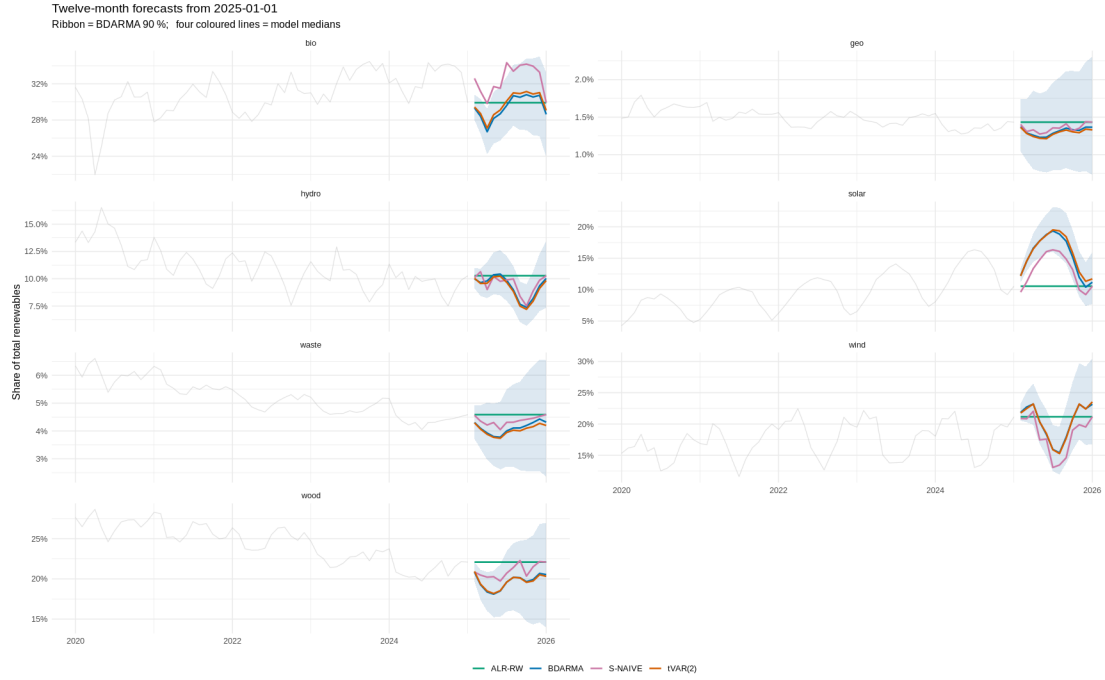


Figure 8: Twelve-month forecasts issued 2025-01-01 after refitting all models to the 2010–2024 sample. Blue shading denotes the BDARMA 90% predictive interval; colored lines are posterior or plug-in *medians*. Axes are free by facet.

depend critically on both the mean mix and its dispersion.

Methodologically the model is straightforward to extend. Exogenous drivers like fuel prices, policy shocks, regional weather indices—can be added as additional columns in the mean or precision design matrices, and the hierarchical structure naturally scales to state or utility sub-regions. Future work may also explore coupling the Dirichlet layer with non-linear latent dynamics or integrating the forecast densities into stochastic power-system optimization. For the present, the results demonstrate that a modest amount of Bayesian structure, applied in the right geometric space, is enough to yield substantial predictive gains and actionable insights for the energy-transition debate.

Acknowledgments

Sean Wilson for insightful discussions and for his invaluable assistance in developing the original *BDARMA* Stan code.

Code Availability

All **R** scripts and **Stan** model files used in this study are publicly available at <https://github.com/harrisonekatz/energy-compositions>. All results and figures in this manuscript can be reproduced by running the scripts found in that repository.

Conflict of Interest

The authors declare no conflicts of interest and that all work and opinions are their own and that the work is not sponsored or endorsed by Airbnb

References

Aitchison, J. (1986). *The Statistical Analysis of Compositional Data*. London: Chapman & Hall.

Aitchison, J. and S. M. Shen (1980). Logistic-normal distributions: Some properties and uses. *Biometrika* 67(2), 261–272.

Billheimer, D., P. Guttorp, and P. Fong (2001). Statistical interpretation of species composition. *Journal of the American Statistical Association* 96(456), 1205–1214.

Chen, C., J. Wang, and T. Hong (2017). Short-term load forecasting using the copy-last-day approach with data cleansing. *IEEE Transactions on Power Systems* 32(5), 3536–3537.

Das, D., S. Rangapuram, K. Benidis, J. Gasthaus, and D. Salinas (2023). Hierarchical probabilistic forecasting with deep dirichlet models. In *Proceedings are UAI 2023 (PMLR 216)*, pp. 13327–13335.

Di Cook, B. Schloerke, et al. (2021). *GGally: Extension to 'ggplot2'*. R package version 2.2.0.

Egozcue, J. J., V. Pawlowsky-Glahn, G. Mateu-Figueras, and C. Barceló-Vidal (2003). Isometric logratio transformations for compositional data analysis. *Mathematical Geology* 35(3), 279–300.

Firke, S. (2023). *janitor: Simple Tools for Examining and Cleaning Dirty Data*. R package version 2.3.2.

Goodrich, B., J. Gabry, P. Bürkner, and R. Češnovar (2024). *rstan: R Interface to Stan*. R package version 2.32.

Grolemund, G. and H. Wickham (2011). *lubridate: Make Dealing with Dates a Little Easier*. R package version 1.9.3.

Harris, T., J. Devkota, V. Khanna, P. Eranki, and A. Landis (2018). Logistic growth curve modeling of us energy production and consumption. *Renewable and Sustainable Energy Reviews* 96, 46–57.

He, Y., Y. Chen, W. Zhang, and Y. Wang (2022). Optimizing energy consumption structure in chongqing of china to achieve low-carbon and sustainable development based on compositional data. *Sustainable Energy Technologies and Assessments* 52, 102340.

Hyndman, R. J. and G. Athanasopoulos (2018). *Forecasting: Principles and Practice* (2nd ed.). OTexts.

International Energy Agency (2024). Renewables 2024. <https://www.iea.org/reports/renewables-2024>. Accessed 24 May 2025.

Kassambara, A. (2022). *ggcorrplot: Visualization of a Correlation Matrix using 'ggplot2'*. R package version 0.1.4.

Katz, H., K. T. Brusch, and R. E. Weiss (2024). A Bayesian Dirichlet ARMA model for forecasting lead times. *International Journal of Forecasting* 40(4), 1556–1567.

Katz, H., L. Medina, and R. E. Weiss (2025). Sensitivity analysis of priors in the Bayesian Dirichlet Auto-Regressive Moving Average Model. *Forecasting* 7(3).

Koopman, S. J., K. Lee, and A. Lucas (2023). Dynamic dirichlet–multinomial modelling of market shares. Discussion Paper TI 2023-039/III, Tinbergen Institute.

Ma, J., A. Oppong, K. Acheampong, and L. Abruquah (2018). Forecasting renewable energy consumption under zero assumptions. *Sustainability* 10(3), 576.

Morais, J., C. Thomas-Agnan, and M. Simioni (2018). Using compositional and dirichlet models for market share regression. *Journal of Applied Statistics* 45(9), 1670–1689.

Panapakidis, I. P. and A. S. Dagoumas (2016). Day-ahead electricity price forecasting via the adaptive neuro-fuzzy inference system. *Energy* 115, 1204–1222.

Pedersen, T. L. (2025). *patchwork: The Composer of Plots*. R package version 1.3.2.

Pfaff, B. (2008). Var, svar and svec models: Implementation within r package vars. *Journal of Statistical Software* 27(4).

Pfaff, B. (2024). *FinTS: Companion to Tsay (2005) Analysis of Financial Time Series*. R package version 0.5-4.

Qian, W., X. Liang, Y. Sun, and L. Tan (2022). A novel adaptive discrete grey prediction model for forecasting development in energy consumption structure—from the perspective of compositional data. *Grey Systems: Theory and Application*. Ahead-of-print.

R Core Team (2024). *R: A Language and Environment for Statistical Computing*. Vienna, Austria: R Foundation for Statistical Computing.

Schuhmacher, D., J. Heinemann, and F. Schmitz (2020). *transport: Computation of Optimal Transport Plans and Wasserstein Distances*. R package version 0.13-2.

Snyder, R. D., J. K. Ord, and A. Beaumont (2017). Forecasting the evolution of the age–sex distribution of consumer loans. *International Journal of Forecasting* 33(3), 695–706.

Stan Development Team (2023). *Stan Modeling Language Users Guide and Reference Manual, Version 2.33*.

Suo, R., Q. Wang, Y. Tan, and Q. Han (2024). An innovative mgm–bpnn–arima model for china’s energy consumption structure forecasting from the perspective of compositional data. *Scientific Reports* 14, 8494.

Tsay, R. S. (2023). *MTS: All-Purpose Toolkit for Multivariate Time Series Analysis*. R package version 1.4.1.

U.S. Energy Information Administration (2024). Electric power monthly, april 2024. <https://www.eia.gov/electricity/monthly/>. Accessed 24 May 2025.

U.S. Energy Information Administration (2025). What is U.S. electricity generation by energy source? <https://www.eia.gov/tools/faqs/faq.php?id=427&t=3>. Accessed 1 July 2025.

van den Boogaart, K. G. and R. Tolosana-Delgado (2024). *compositions: Compositional Data Analysis*. R package version 2.0-8.

Wei, Y., Z. Wang, H. Wang, and Y. Li (2021). Compositional data techniques for forecasting dynamic change in china’s energy consumption structure by 2020 and 2030. *Journal of Cleaner Production* 284, 124702.

Wickham, H. et al. (2019). Welcome to the tidyverse. *Journal of Open Source Software* 4(43), 1686.

Wickham, H. and D. Seidel (2019). *scales: Scale Functions for Visualization*. R package version 1.3.0.

Xiao, X. and X. Li (2023). A novel compositional data model for predicting the energy consumption structures of europe, japan, and china. *Environment, Development and Sustainability* 25(10), 11673–11698.

Xu, C., X. Xiao, and H. Chen (2024). A novel method for forecasting renewable energy consumption structure based on compositional data: evidence from china, the usa, and canada. *Environment, Development and Sustainability* 26(2), 5299–5333.

Zhang, K., K. Yin, and W. Yang (2022). Predicting bio-energy power-generation structure using a newly developed grey compositional data model: A case study in china. *Renewable Energy* 198, 695–711.

Zheng, X., G. Lin, and J. Chen (2017). Dirichlet autoregressive moving average models for compositional time series. *Journal of Statistical Computation and Simulation* 87(16), 3217–3234.

Zhu, Z. (2021). *kableExtra: Construct Complex Table with 'kable' and Pipe Syntax*. R package version 1.3.4.